

Received November 27, 2020, accepted December 9, 2020, date of publication December 14, 2020, date of current version December 30, 2020.

Digital Object Identifier 10.1109/ACCESS.2020.3044548

# Optimal Type-3 Fuzzy System for Solving Singular Multi-Pantograph Equations

CHAO MA<sup>1</sup>, ARDASHIR MOHAMMADZADEH<sup>2</sup>, HAMZA TURABIEH<sup>3</sup>, MAJDI MAFARJA<sup>4</sup>, SHAHAB S. BAND<sup>5</sup>, AND AMIR MOSAVI<sup>6,7,8,9</sup>

<sup>1</sup>School of Digital Media, Shenzhen Institute of Information Technology, Shenzhen 518172, China

<sup>2</sup>Department of Electrical Engineering, Faculty of Engineering, University of Bonab, Bonab 5551785176, Iran

<sup>3</sup>Department of Information Technology, College of Computers and Information Technology, Taif University, Taif 21944, Saudi Arabia

<sup>4</sup>Department of Computer Science, Birzeit University, Birzeit 72439, Palestine

<sup>5</sup>Future Technology Research Center, College of Future, National Yunlin University of Science and Technology 123 University Road, Section 3, Douliou, Yunlin 64002, Taiwan, R.O.C.

<sup>6</sup>John von Neumann Faculty of Informatics, Obuda University, 1034 Budapest, Hungary

<sup>7</sup>School of Economics and Business, Norwegian University of Life Sciences, 1430 Ås, Norway

<sup>8</sup>Department of Informatics, J. Selye University, 94501 Komarno, Slovakia

<sup>9</sup>School of the Built Environment, Oxford Brookes University, Oxford OX3 0BP, U.K.

Corresponding authors: Amir Mosavi (amir.mosavi@kvk.uni-obuda.hu) and Shahab S. Band (shamshirbands@yuntech.edu.tw)

This work was supported by the Taif University Researchers Supporting Project Number (TURSP-2020/125), Taif University, Taif, Saudi Arabia. Also it is supported by the characteristic innovation Project of Guangdong University 2020 (2020KTSCX302).

**ABSTRACT** In this study a new machine learning technique is presented to solve singular multi-pantograph differential equations (SMDEs). A new optimized type-3 fuzzy logic system (T3-FLS) by unscented Kalman filter (UKF) is proposed for solution estimation. The convergence and stability of presented algorithm are ensured by the suggested Lyapunov analysis. By two SMDEs the effectiveness and applicability of the suggested method is demonstrated. The statistical analysis show that the suggested method results in accurate and robust performance and the estimated solution is well converged to the exact solution. The proposed algorithm is simple and can be applied on various SMDEs with variable coefficients.

**INDEX TERMS** Machine learning, artificial intelligence, fuzzy systems, Lyapunov stability, learning algorithm, multi-pantograph differential equations.

## I. INTRODUCTION

The numerical solving of singular multi-pantograph differential equations (SMDEs) has been one of the interesting research topic, due to the potential application of SMDEs in various science field such as: electrodynamics, quantum mechanics, chemical engineering, astrophysics and many others [1], [2].

Many numerical techniques have been designed for solving SMDEs. For example, Jiang *et al.* [2] propose Galerkin method for solving of SMDE and the global convergence is studied. In [1], by the use of variational theorem and Laplace transform the analytical solution is estimated. A numerical method on basis of the multistage homotopy technique has also been suggested and its accuracy has been examined [3]. Bilal *et al.* [4], present the Boubeker polynomial approach to construct a numerical solver for SMDEs and its convergence is studied. In [5], the Legendre–Gauss collocation approach is presented in contrast to Hermite collocation

The associate editor coordinating the review of this manuscript and approving it for publication was Jianquan Lu.

method and its versatility and convergence are examined. Doha *et al.* [6], suggest the Jacobi rational-Gauss function and a semi-analytical method. In [7], by the use of Adams and Runge–Kutta methods a numerical technique is developed and its performance is evaluated by some numerical examples. In [8], the reduction of SMDEs into algebraic equations using Chelyshkov wavelet basis is studied and then by the use of Galerkin approach a solver is proposed. Rayal and Verma [9], propose Legendre wavelet to solve SMDEs and the behaviour of SMDEs using different fractional derivative definitions is studied.

One of the recently developed approach for solving differential equations is the use of intelligent systems and learning techniques [10]. Combination of fuzzy logic systems (FLSs) and learning methods is applied in wide engineering problems, due to the strong capability of this approach [11]–[17]. However, on the best knowledge of authors, this powerful tool has not been applied for solving SMDEs. However, quite rarely techniques on basis neural networks (NNs) have been applied on solving a simple class of differential equations. For example, in [18], NNs and evolutionary based algorithms

such as genetic and pattern search algorithms are employed to solve pantograph differential equations (PDE). Similar to [18], in [19], interior-point method is combined with NNs to find a solution for PDEs. In [20], the Lagaris method is developed to estimate the real solution of PDEs by a simple NN. In [21], NNs are used to solve Painlevé equations and the effectiveness of NNs is shown. In [22], similar to above mentioned approaches, the solving of a class of differential equations by NN is investigated and the genetic algorithm is used to optimize NNs.

In the most of above reviewed NN based solvers, only PDEs have been studied and the singular PDEs needs more studies. Also in the most of NN based solvers, evolutionary methods have been used that are not suitable for online applications and also these algorithms suffer heavy computational cost. Furthermore, in the most of the aforementioned numerical methods the stability is not guaranteed. Recently, it has been shown in literature that FLSs, specially high-order FLSs have more capability than NNs. In various engineering applications the superiority of type-2 and type-3 FLSs have been shown such as: decision making [23], control systems [24], identification [25], chaotic synchronization [26], multi-agent control systems [27], among many others.

In addition to structure of NN and FLS, the optimization and learning approaches are also important in effectiveness. Many optimization methods have been developed for learning of NNs and various applications such as kernel extreme learning, support vector machine, chaotic optimization, bacterial foraging optimization, among many others [28]–[35]. The UKF algorithm is also widely used in many nonlinear problems [36]–[38], because of its more accurate performance. However, literature review shows that UKF has been rarely used in optimization of FLSs and problem of SMDEs.

Considering above motivations, in this study, a new approach on criteria of T3-FLSs and UKF algorithm is presented for solution approximation of SMDEs. By the several statistical examinations the well performance of the suggested solver is demonstrated. The main contributions are:

- A new approach is presented to solve SMDEs.
- For the best knowledge of authors, for the first time a T3-FLS approach is presented for solving SMDEs.
- A new cost function and a new learning algorithm are presented to optimize the suggested T3-FLS based solver.
- The closed-loop stability is proved.
- Several statistical analysis is presented to examine the accuracy and robustness of the suggested T3-FLS based solver.

## II. PROBLEM DESCRIPTION

The suggested approach designs FLSs and UKF algorithm. A general view on suggested solution method is depicted in Fig. 1. A SMDE is given as:

$$\ddot{x}(t) + \sum_{k=1}^n \dot{x}(r_k t) / P_k(t) + x(t) / Q_k = G(t) \quad (1)$$

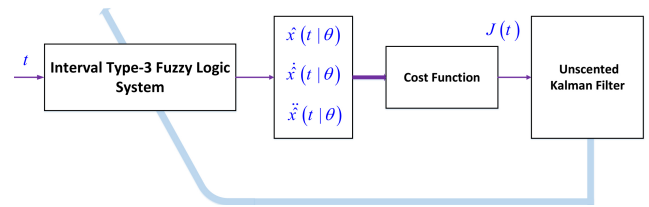


FIGURE 1. A general view of the proposed solver.

where  $x(0) = A_1$  and  $\dot{x}(0) = A_2$ .  $P_k(t)$  and  $G(t)$  are continues function. The objective is tuning the parameters of T3-FLS such that the output of T3-FLS  $\hat{x}(t)$  to be converged to  $x(t)$ . Then the following equation is solved:

$$\ddot{\hat{x}}(t) + \sum_{k=1}^n \dot{\hat{x}}(r_k t) / P_k(t) + \hat{x}(t) / Q_k = G(t) \quad (2)$$

To solve (2), the following cost function is considered:

$$J = \frac{1}{N} \sum_{i=1}^N \left( \ddot{\hat{x}}_i(t) + \sum_{k=1}^n \dot{\hat{x}}_i(r_k t) / P_{k,i}(t) + \hat{x}_i(t) / Q_i - G(t) \right)^2 + \frac{1}{2} (\hat{x}_0^2 + \dot{\hat{x}}_0^2) \quad (3)$$

where  $i = 1, \dots, N, k = 1, \dots, n, Nh = 1$  and  $t = kh$ .

*Remark 1:* It should be noted that, the Volterra integral equations can be considered as a special case of multi-pantographic differential equations (see [39]–[41]).

The problem is that the parameters of T3-FLS are tuned such that (3) to be minimized and the convergence error to be stable. The parameters are of T3-FLS are tuned through the UKF algorithm and the convergence is ensured by Lyapunov method.

## III. TYPE-3 FLS

In this section the suggested T3-FLS solution estimator is illustrated. The suggested structure is depicted in Fig. 2. The computations are explained as follows. 1) For input,  $M$  type-3 membership function (MF)  $\tilde{A}_{l|\alpha}$  as shown in Fig. 3 is considered. Each MF is divided into  $\iota$   $\alpha$ -cuts.

2) Compute the rule firings:

$$\bar{\psi}_{\bar{\alpha}_j}^l(u) = \exp\left(-\left(u - c_{\tilde{A}_{l|\alpha}}\right)^2 / \bar{\vartheta}_{\tilde{A}_{l|\bar{\alpha}_j}}^2\right) \quad (4)$$

$$\bar{\psi}_{\alpha_j}^l(u) = \exp\left(-\left(u - c_{\tilde{A}_{l|\alpha}}\right)^2 / \bar{\vartheta}_{\tilde{A}_{l|\alpha_j}}^2\right) \quad (5)$$

$$\underline{\psi}_{\bar{\alpha}_j}^l(u) = \exp\left(-\left(u - c_{\tilde{A}_{l|\alpha}}\right)^2 / \underline{\vartheta}_{\tilde{A}_{l|\bar{\alpha}_j}}^2\right) \quad (6)$$

$$\underline{\psi}_{\alpha_j}^l(u) = \exp\left(-\left(u - c_{\tilde{A}_{l|\alpha}}\right)^2 / \underline{\vartheta}_{\tilde{A}_{l|\alpha_j}}^2\right) \quad (7)$$

where  $l = 1, \dots, M, \bar{\alpha} \in \bar{\alpha}_1, \dots, \bar{\alpha}_\iota, \alpha \in \alpha_1, \dots, \alpha_\iota, c_{\tilde{A}_{l|\alpha}}$  and  $c_{\tilde{A}_{l|\alpha}}$  are the center of  $\tilde{A}_{l|\alpha}$ ,  $\bar{\vartheta}_{\tilde{A}_{l|\bar{\alpha}_j}}$  and  $\bar{\vartheta}_{\tilde{A}_{l|\alpha_j}}$  are the upper standard divisions at upper and lower  $\alpha$ -cut, respectively,  $\underline{\vartheta}_{\tilde{A}_{l|\bar{\alpha}_j}}$  and  $\underline{\vartheta}_{\tilde{A}_{l|\alpha_j}}$  are the lower standard divisions at upper and

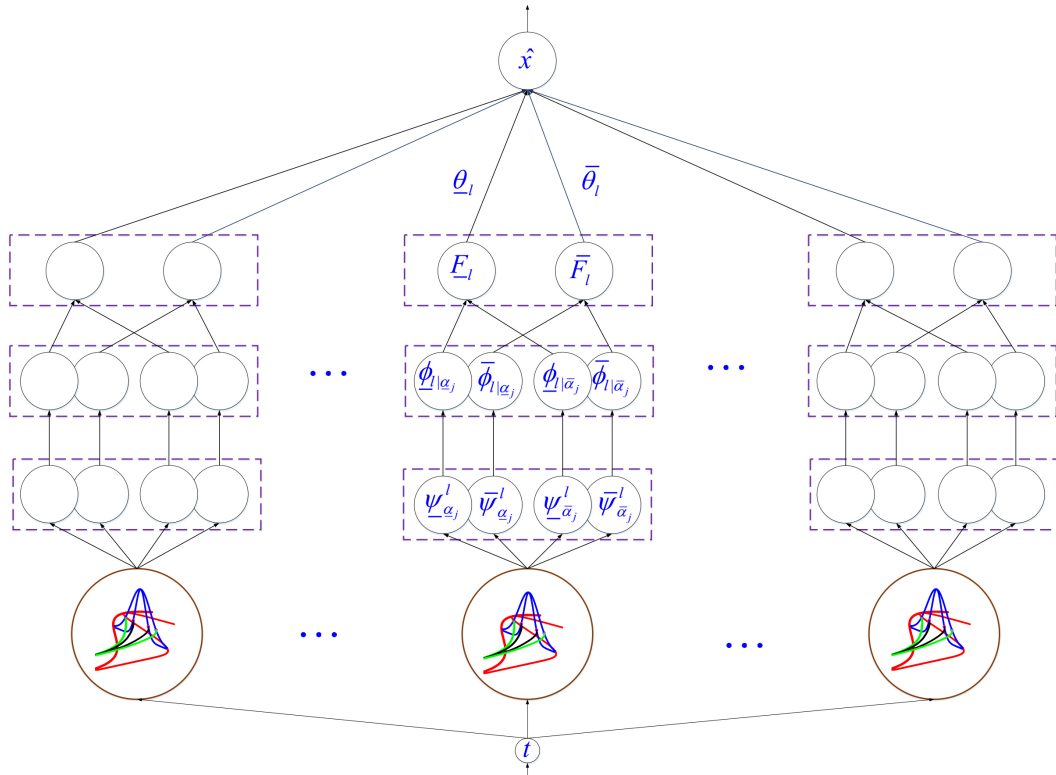


FIGURE 2. A general view of the proposed T3-FLS solution estimator.

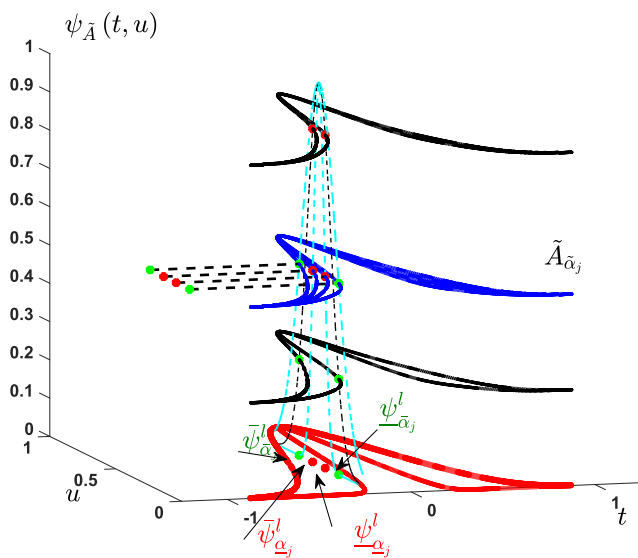


FIGURE 3. Suggested type-3 MF.

lower  $\alpha$ -cut, respectively. 3) Compute the normalized rule firing (first type-reduction):

$$\bar{\phi}_{l|\bar{\alpha}_j} = \frac{\bar{\psi}_{\bar{\alpha}_j}^l}{\sum_{l=1}^M (\bar{\psi}_{\bar{\alpha}_j}^l + \psi_{\bar{\alpha}_j}^l)} \quad (8)$$

$$\bar{\phi}_{l|\alpha_j} = \frac{\bar{\psi}_{\alpha_j}^l}{\sum_{l=1}^M (\bar{\psi}_{\alpha_j}^l + \psi_{\alpha_j}^l)} \quad (9)$$

$$\phi_{l|\bar{\alpha}_j} = \frac{\psi_{\bar{\alpha}_j}^l}{\sum_{l=1}^M (\psi_{\bar{\alpha}_j}^l + \bar{\psi}_{\bar{\alpha}_j}^l)} \quad (10)$$

$$\phi_{l|\alpha_j} = \frac{\psi_{\alpha_j}^l}{\sum_{l=1}^M (\psi_{\alpha_j}^l + \bar{\psi}_{\alpha_j}^l)} \quad (11)$$

4) Compute the second type-reduction:

$$\begin{aligned} \bar{F}_l &= \frac{\sum_{j=1}^l \bar{\alpha}_j \bar{\phi}_{l|\bar{\alpha}_j}}{\sum_{j=1}^l (\bar{\alpha}_j + \alpha_j)} \\ &+ \frac{\sum_{j=1}^l \alpha_j \bar{\phi}_{l|\alpha_j}}{\sum_{j=1}^l (\bar{\alpha}_j + \alpha_j)}, \quad l = 1, \dots, M \end{aligned} \quad (12)$$

$$\begin{aligned} F_l &= \frac{\sum_{j=1}^l \bar{\alpha}_j \phi_{l|\bar{\alpha}_j}}{\sum_{j=1}^l (\bar{\alpha}_j + \alpha_j)} \\ &+ \frac{\sum_{j=1}^l \alpha_j \phi_{l|\alpha_j}}{\sum_{j=1}^l (\bar{\alpha}_j + \alpha_j)}, \quad l = 1, \dots, M \end{aligned} \quad (13)$$

5) Compute output as:

$$\begin{aligned} \hat{x}(u, \theta) &= \theta^T F(u), \\ \theta &= [\underline{\theta}_1, \dots, \underline{\theta}_M, \bar{\theta}_1, \dots, \bar{\theta}_M]^T \\ F(u) &= [\underline{F}_1, \dots, \underline{F}_M, \bar{F}_1, \dots, \bar{F}_M]^T \end{aligned} \quad (14)$$

where  $\theta$  represents the vector of trainable parameters. From (14),  $\hat{x}(u, \theta)$  is obtained as:

$$\dot{\hat{x}}(u, \theta) = \frac{\partial \hat{x}(u, \theta)}{\partial u} = \theta^T \frac{\partial F(u)}{\partial u} \quad (15)$$

where

$$\frac{\partial F(u)}{\partial u} = \left[ \frac{\partial \underline{F}_1}{\partial u}, \dots, \frac{\partial \underline{F}_M}{\partial u}, \frac{\partial \bar{F}_1}{\partial u}, \dots, \frac{\partial \bar{F}_M}{\partial u} \right]^T \quad (16)$$

From (15), for  $\frac{\partial \underline{F}_l}{\partial u}$  and  $\frac{\partial \bar{F}_l}{\partial u}$ , one has:

$$\begin{aligned} \frac{\partial \underline{F}_l}{\partial u} &= \frac{\sum_{j=1}^l \bar{\alpha}_j \frac{\partial \phi_{l|\bar{\alpha}_j}}{\partial u}}{\sum_{j=1}^l (\bar{\alpha}_j + \alpha_j)} \\ &+ \frac{\sum_{j=1}^l \alpha_j \frac{\partial \phi_{l|\alpha_j}}{\partial u}}{\sum_{j=1}^l (\bar{\alpha}_j + \alpha_j)}, \quad l = 1, \dots, M \end{aligned} \quad (17)$$

$$\begin{aligned} \frac{\partial \bar{F}_l}{\partial u} &= \frac{\sum_{j=1}^l \bar{\alpha}_j \frac{\partial \bar{\phi}_{l|\bar{\alpha}_j}}{\partial u}}{\sum_{j=1}^l (\bar{\alpha}_j + \alpha_j)} \\ &+ \frac{\sum_{j=1}^l \alpha_j \frac{\partial \bar{\phi}_{l|\alpha_j}}{\partial u}}{\sum_{j=1}^l (\bar{\alpha}_j + \alpha_j)}, \quad l = 1, \dots, M \end{aligned} \quad (18)$$

From (17) and (18), the terms  $\frac{\partial \phi_{l|\bar{\alpha}_j}}{\partial u}$ ,  $\frac{\partial \bar{\phi}_{l|\bar{\alpha}_j}}{\partial u}$ ,  $\frac{\partial \phi_{l|\alpha_j}}{\partial u}$  and  $\frac{\partial \bar{\phi}_{l|\alpha_j}}{\partial u}$ , are computed as:

$$\begin{aligned} \frac{\partial \phi_{l|\bar{\alpha}_j}}{\partial u} &= \frac{-2(u - c_{\bar{\lambda}_{l|\alpha}}) / \bar{\vartheta}_{\bar{\lambda}_{l|\alpha}}^2 \bar{\psi}_{\bar{\alpha}_j}^l \sum_{l=1}^M (\bar{\psi}_{\bar{\alpha}_j}^l + \psi_{\bar{\alpha}_j}^l)}{\left[ \sum_{l=1}^M (\bar{\psi}_{\bar{\alpha}_j}^l + \psi_{\bar{\alpha}_j}^l) \right]^2} \\ &- \frac{\bar{\psi}_{\bar{\alpha}_j}^l \sum_{l=1}^M 2(u - c_{\bar{\lambda}_{l|\alpha}}) \left[ \bar{\psi}_{\bar{\alpha}_j}^l / \bar{\vartheta}_{\bar{\lambda}_{l|\alpha}}^2 + \psi_{\bar{\alpha}_j}^l / \vartheta_{\bar{\lambda}_{l|\alpha}}^2 \right]}{\left[ \sum_{r=1}^M (\bar{\psi}_{\bar{\alpha}_j}^l + \psi_{\bar{\alpha}_j}^l) \right]^2} \end{aligned} \quad (19)$$

$$\begin{aligned} \frac{\partial \bar{\phi}_{l|\alpha_j}}{\partial u} &= \frac{-2(u - c_{\bar{\lambda}_{l|\alpha}}) / \bar{\vartheta}_{\bar{\lambda}_{l|\alpha}}^2 \bar{\psi}_{\alpha_j}^l \sum_{l=1}^M (\bar{\psi}_{\alpha_j}^l + \psi_{\alpha_j}^l)}{\left[ \sum_{l=1}^M (\bar{\psi}_{\alpha_j}^l + \psi_{\alpha_j}^l) \right]^2} \\ &- \frac{\bar{\psi}_{\alpha_j}^l \sum_{l=1}^M 2(u - c_{\bar{\lambda}_{l|\alpha}}) \left[ \bar{\psi}_{\alpha_j}^l / \bar{\vartheta}_{\bar{\lambda}_{l|\alpha}}^2 + \psi_{\alpha_j}^l / \vartheta_{\bar{\lambda}_{l|\alpha}}^2 \right]}{\left[ \sum_{r=1}^M (\bar{\psi}_{\alpha_j}^l + \psi_{\alpha_j}^l) \right]^2} \end{aligned} \quad (20)$$

$$\begin{aligned} \frac{\partial \phi_{l|\bar{\alpha}_j}}{\partial u} &= \frac{-2(u - c_{\bar{\lambda}_{l|\alpha}}) / \vartheta_{\bar{\lambda}_{l|\alpha}}^2 \psi_{\bar{\alpha}_j}^l \sum_{l=1}^M (\bar{\psi}_{\bar{\alpha}_j}^l + \psi_{\bar{\alpha}_j}^l)}{\left[ \sum_{l=1}^M (\bar{\psi}_{\bar{\alpha}_j}^l + \psi_{\bar{\alpha}_j}^l) \right]^2} \\ &- \frac{\psi_{\bar{\alpha}_j}^l \sum_{l=1}^M 2(u - c_{\bar{\lambda}_{l|\alpha}}) \left[ \bar{\psi}_{\bar{\alpha}_j}^l / \bar{\vartheta}_{\bar{\lambda}_{l|\alpha}}^2 + \psi_{\bar{\alpha}_j}^l / \vartheta_{\bar{\lambda}_{l|\alpha}}^2 \right]}{\left[ \sum_{r=1}^M (\bar{\psi}_{\bar{\alpha}_j}^l + \psi_{\bar{\alpha}_j}^l) \right]^2} \end{aligned} \quad (21)$$

$$\begin{aligned} \frac{\partial \phi_{l|\alpha_j}}{\partial u} &= \frac{-2(u - c_{\bar{\lambda}_{l|\alpha}}) / \vartheta_{\bar{\lambda}_{l|\alpha}}^2 \psi_{\alpha_j}^l \sum_{l=1}^M (\bar{\psi}_{\alpha_j}^l + \psi_{\alpha_j}^l)}{\left[ \sum_{l=1}^M (\bar{\psi}_{\alpha_j}^l + \psi_{\alpha_j}^l) \right]^2} \\ &- \frac{\psi_{\alpha_j}^l \sum_{l=1}^M 2(u - c_{\bar{\lambda}_{l|\alpha}}) \left[ \bar{\psi}_{\alpha_j}^l / \bar{\vartheta}_{\bar{\lambda}_{l|\alpha}}^2 + \psi_{\alpha_j}^l / \vartheta_{\bar{\lambda}_{l|\alpha}}^2 \right]}{\left[ \sum_{r=1}^M (\bar{\psi}_{\alpha_j}^l + \psi_{\alpha_j}^l) \right]^2} \end{aligned} \quad (22)$$

Similarly, from (15),  $\ddot{\hat{x}}(t)$  is computed as:

$$\ddot{\hat{x}}(u, \theta) = \frac{\partial \dot{\hat{x}}(u, \theta)}{\partial u} = \theta^T \frac{\partial \dot{F}(u)}{\partial u} \quad (23)$$

where

$$\frac{\partial \dot{F}(u)}{\partial u} = \left[ \frac{\partial \dot{\underline{F}}_1}{\partial u}, \dots, \frac{\partial \dot{\underline{F}}_M}{\partial u}, \frac{\partial \dot{\bar{F}}_1}{\partial u}, \dots, \frac{\partial \dot{\bar{F}}_M}{\partial u} \right] \quad (24)$$

From (24),  $\frac{\partial \dot{\underline{F}}_l}{\partial u}$  and  $\frac{\partial \dot{\bar{F}}_l}{\partial u}$ , are computed as:

$$\begin{aligned} \frac{\partial \dot{\underline{F}}_l}{\partial u} &= \frac{\sum_{j=1}^l \bar{\alpha}_j \frac{\partial \dot{\phi}_{l|\bar{\alpha}_j}}{\partial u}}{\sum_{j=1}^l (\bar{\alpha}_j + \alpha_j)} \\ &+ \frac{\sum_{j=1}^l \alpha_j \frac{\partial \dot{\phi}_{l|\alpha_j}}{\partial u}}{\sum_{j=1}^l (\bar{\alpha}_j + \alpha_j)}, \quad l = 1, \dots, M \end{aligned} \quad (25)$$

$$\frac{\partial \dot{F}_l}{\partial u} = \frac{\sum_{j=1}^l \bar{\alpha}_j \frac{\partial \dot{\phi}_{l|\bar{\alpha}_j}}{\partial u}}{\sum_{j=1}^l (\bar{\alpha}_j + \underline{\alpha}_j)} + \frac{\sum_{j=1}^l \underline{\alpha}_j \frac{\partial \dot{\phi}_{l|\underline{\alpha}_j}}{\partial u}}{\sum_{j=1}^l (\bar{\alpha}_j + \underline{\alpha}_j)}, \quad l = 1, \dots, M \quad (26)$$

where  $\frac{\partial \dot{\phi}_{l|\bar{\alpha}_j}}{\partial u}$ ,  $\frac{\partial \dot{\phi}_{l|\underline{\alpha}_j}}{\partial u}$ ,  $\frac{\partial \dot{\phi}_{l|\bar{\alpha}_j}}{\partial u}$  and  $\frac{\partial \dot{\phi}_{l|\underline{\alpha}_j}}{\partial u}$ , are computed as:

$$\frac{\partial \dot{\phi}_{l|\bar{\alpha}_j}}{\partial u} = \frac{\left\{ \begin{array}{l} \frac{-2u}{\bar{\vartheta}_{\bar{A}_{l|\bar{\alpha}_j}}^2} \bar{\psi}_{\bar{\alpha}_j}^l \sum_{l=1}^M (\bar{\psi}_{\bar{\alpha}_j}^l + \underline{\psi}_{\bar{\alpha}_j}^l) - 2(u - c_{\bar{A}_{l|\bar{\alpha}_j}}) / \bar{\vartheta}_{\bar{A}_{l|\bar{\alpha}_j}}^2 \cdot \\ \left[ -2(u - c_{\bar{A}_{l|\bar{\alpha}_j}}) / \bar{\vartheta}_{\bar{A}_{l|\bar{\alpha}_j}}^2 \bar{\psi}_{\bar{\alpha}_j}^l \sum_{l=1}^M (\bar{\psi}_{\bar{\alpha}_j}^l + \underline{\psi}_{\bar{\alpha}_j}^l) + \right. \\ \left. \bar{\psi}_{\bar{\alpha}_j}^l \sum_{l=1}^M 2(u - c_{\bar{A}_{l|\bar{\alpha}_j}}) \left[ \bar{\psi}_{\bar{\alpha}_j}^l / \bar{\vartheta}_{\bar{A}_{l|\bar{\alpha}_j}}^2 + \underline{\psi}_{\bar{\alpha}_j}^l / \bar{\vartheta}_{\bar{A}_{l|\bar{\alpha}_j}}^2 \right] \right] \end{array} \right\}}{\left[ \sum_{l=1}^M (\bar{\psi}_{\bar{\alpha}_j}^l + \underline{\psi}_{\bar{\alpha}_j}^l) \right]^2} \\ = \frac{\left\{ \begin{array}{l} -2(u - c_{\bar{A}_{l|\bar{\alpha}_j}}) / \bar{\vartheta}_{\bar{A}_{l|\bar{\alpha}_j}}^2 \bar{\psi}_{\bar{\alpha}_j}^l \sum_{l=1}^M (\bar{\psi}_{\bar{\alpha}_j}^l + \underline{\psi}_{\bar{\alpha}_j}^l) \cdot \\ \left[ \sum_{l=1}^M 2(u - c_{\bar{A}_{l|\bar{\alpha}_j}}) \left[ \bar{\psi}_{\bar{\alpha}_j}^l / \bar{\vartheta}_{\bar{A}_{l|\bar{\alpha}_j}}^2 + \underline{\psi}_{\bar{\alpha}_j}^l / \bar{\vartheta}_{\bar{A}_{l|\bar{\alpha}_j}}^2 \right] \right] \end{array} \right\}}{\left[ \sum_{l=1}^M (\bar{\psi}_{\bar{\alpha}_j}^l + \underline{\psi}_{\bar{\alpha}_j}^l) \right]^4} \quad (27)$$

$$\frac{\partial \dot{\phi}_{l|\underline{\alpha}_j}}{\partial u} = \frac{\left\{ \begin{array}{l} \frac{-2u}{\bar{\vartheta}_{\bar{A}_{l|\underline{\alpha}_j}}^2} \bar{\psi}_{\underline{\alpha}_j}^l \sum_{l=1}^M (\bar{\psi}_{\underline{\alpha}_j}^l + \underline{\psi}_{\underline{\alpha}_j}^l) - 2(u - c_{\bar{A}_{l|\underline{\alpha}_j}}) / \bar{\vartheta}_{\bar{A}_{l|\underline{\alpha}_j}}^2 \cdot \\ \left[ -2(u - c_{\bar{A}_{l|\underline{\alpha}_j}}) / \bar{\vartheta}_{\bar{A}_{l|\underline{\alpha}_j}}^2 \bar{\psi}_{\underline{\alpha}_j}^l \sum_{l=1}^M (\bar{\psi}_{\underline{\alpha}_j}^l + \underline{\psi}_{\underline{\alpha}_j}^l) + \right. \\ \left. \bar{\psi}_{\underline{\alpha}_j}^l \sum_{l=1}^M 2(u - c_{\bar{A}_{l|\underline{\alpha}_j}}) \left[ \bar{\psi}_{\underline{\alpha}_j}^l / \bar{\vartheta}_{\bar{A}_{l|\underline{\alpha}_j}}^2 + \underline{\psi}_{\underline{\alpha}_j}^l / \bar{\vartheta}_{\bar{A}_{l|\underline{\alpha}_j}}^2 \right] \right] \end{array} \right\}}{\left[ \sum_{l=1}^M (\bar{\psi}_{\underline{\alpha}_j}^l + \underline{\psi}_{\underline{\alpha}_j}^l) \right]^2} \\ = \frac{\left\{ \begin{array}{l} -2(u - c_{\bar{A}_{l|\underline{\alpha}_j}}) / \bar{\vartheta}_{\bar{A}_{l|\underline{\alpha}_j}}^2 \bar{\psi}_{\underline{\alpha}_j}^l \sum_{l=1}^M (\bar{\psi}_{\underline{\alpha}_j}^l + \underline{\psi}_{\underline{\alpha}_j}^l) \cdot \\ \left[ \sum_{l=1}^M 2(u - c_{\bar{A}_{l|\underline{\alpha}_j}}) \left[ \bar{\psi}_{\underline{\alpha}_j}^l / \bar{\vartheta}_{\bar{A}_{l|\underline{\alpha}_j}}^2 + \underline{\psi}_{\underline{\alpha}_j}^l / \bar{\vartheta}_{\bar{A}_{l|\underline{\alpha}_j}}^2 \right] \right] \end{array} \right\}}{\left[ \sum_{l=1}^M (\bar{\psi}_{\underline{\alpha}_j}^l + \underline{\psi}_{\underline{\alpha}_j}^l) \right]^4} \quad (28)$$

$$\frac{\partial \dot{\phi}_{l|\bar{\alpha}_j}}{\partial u} = \frac{\left\{ \begin{array}{l} \frac{-2u}{\bar{\vartheta}_{\bar{A}_{l|\bar{\alpha}_j}}^2} \bar{\psi}_{\bar{\alpha}_j}^l \sum_{l=1}^M (\bar{\psi}_{\bar{\alpha}_j}^l + \underline{\psi}_{\bar{\alpha}_j}^l) - 2(u - c_{\bar{A}_{l|\bar{\alpha}_j}}) / \bar{\vartheta}_{\bar{A}_{l|\bar{\alpha}_j}}^2 \cdot \\ \left[ -2(u - c_{\bar{A}_{l|\bar{\alpha}_j}}) / \bar{\vartheta}_{\bar{A}_{l|\bar{\alpha}_j}}^2 \bar{\psi}_{\bar{\alpha}_j}^l \sum_{l=1}^M (\bar{\psi}_{\bar{\alpha}_j}^l + \underline{\psi}_{\bar{\alpha}_j}^l) + \right. \\ \left. \bar{\psi}_{\bar{\alpha}_j}^l \sum_{l=1}^M 2(u - c_{\bar{A}_{l|\bar{\alpha}_j}}) \left[ \bar{\psi}_{\bar{\alpha}_j}^l / \bar{\vartheta}_{\bar{A}_{l|\bar{\alpha}_j}}^2 + \underline{\psi}_{\bar{\alpha}_j}^l / \bar{\vartheta}_{\bar{A}_{l|\bar{\alpha}_j}}^2 \right] \right] \end{array} \right\}}{\left[ \sum_{l=1}^M (\bar{\psi}_{\bar{\alpha}_j}^l + \underline{\psi}_{\bar{\alpha}_j}^l) \right]^2} \\ = \frac{\left\{ \begin{array}{l} -2(u - c_{\bar{A}_{l|\bar{\alpha}_j}}) / \bar{\vartheta}_{\bar{A}_{l|\bar{\alpha}_j}}^2 \bar{\psi}_{\bar{\alpha}_j}^l \sum_{l=1}^M (\bar{\psi}_{\bar{\alpha}_j}^l + \underline{\psi}_{\bar{\alpha}_j}^l) \cdot \\ \left[ \sum_{l=1}^M 2(u - c_{\bar{A}_{l|\bar{\alpha}_j}}) \left[ \bar{\psi}_{\bar{\alpha}_j}^l / \bar{\vartheta}_{\bar{A}_{l|\bar{\alpha}_j}}^2 + \underline{\psi}_{\bar{\alpha}_j}^l / \bar{\vartheta}_{\bar{A}_{l|\bar{\alpha}_j}}^2 \right] \right] \end{array} \right\}}{\left[ \sum_{l=1}^M (\bar{\psi}_{\bar{\alpha}_j}^l + \underline{\psi}_{\bar{\alpha}_j}^l) \right]^4} \quad (29)$$

$$\frac{\partial \dot{\phi}_{l|\underline{\alpha}_j}}{\partial u} = \frac{\left\{ \begin{array}{l} \frac{-2u}{\bar{\vartheta}_{\bar{A}_{l|\underline{\alpha}_j}}^2} \bar{\psi}_{\underline{\alpha}_j}^l \sum_{l=1}^M (\bar{\psi}_{\underline{\alpha}_j}^l + \underline{\psi}_{\underline{\alpha}_j}^l) - 2(u - c_{\bar{A}_{l|\underline{\alpha}_j}}) / \bar{\vartheta}_{\bar{A}_{l|\underline{\alpha}_j}}^2 \cdot \\ \left[ -2(u - c_{\bar{A}_{l|\underline{\alpha}_j}}) / \bar{\vartheta}_{\bar{A}_{l|\underline{\alpha}_j}}^2 \bar{\psi}_{\underline{\alpha}_j}^l \sum_{l=1}^M (\bar{\psi}_{\underline{\alpha}_j}^l + \underline{\psi}_{\underline{\alpha}_j}^l) + \right. \\ \left. \bar{\psi}_{\underline{\alpha}_j}^l \sum_{l=1}^M 2(u - c_{\bar{A}_{l|\underline{\alpha}_j}}) \left[ \bar{\psi}_{\underline{\alpha}_j}^l / \bar{\vartheta}_{\bar{A}_{l|\underline{\alpha}_j}}^2 + \underline{\psi}_{\underline{\alpha}_j}^l / \bar{\vartheta}_{\bar{A}_{l|\underline{\alpha}_j}}^2 \right] \right] \end{array} \right\}}{\left[ \sum_{l=1}^M (\bar{\psi}_{\underline{\alpha}_j}^l + \underline{\psi}_{\underline{\alpha}_j}^l) \right]^2} \\ = \frac{\left\{ \begin{array}{l} -2(u - c_{\bar{A}_{l|\underline{\alpha}_j}}) / \bar{\vartheta}_{\bar{A}_{l|\underline{\alpha}_j}}^2 \bar{\psi}_{\underline{\alpha}_j}^l \sum_{l=1}^M (\bar{\psi}_{\underline{\alpha}_j}^l + \underline{\psi}_{\underline{\alpha}_j}^l) \cdot \\ \left[ \sum_{l=1}^M 2(u - c_{\bar{A}_{l|\underline{\alpha}_j}}) \left[ \bar{\psi}_{\underline{\alpha}_j}^l / \bar{\vartheta}_{\bar{A}_{l|\underline{\alpha}_j}}^2 + \underline{\psi}_{\underline{\alpha}_j}^l / \bar{\vartheta}_{\bar{A}_{l|\underline{\alpha}_j}}^2 \right] \right] \end{array} \right\}}{\left[ \sum_{l=1}^M (\bar{\psi}_{\underline{\alpha}_j}^l + \underline{\psi}_{\underline{\alpha}_j}^l) \right]^4} \quad (30)$$

IV. LEARNING METHOD

The parameters are of T3-FLS are tuned through the UKF algorithm. To apply UKF algorithm, the following state-space model is considered:

$$w(t+1) = w(t) + \psi(t) \\ v(w(t+1), t+1) = v(w(t), t) + \chi(t) \quad (31)$$

where

$$v(w, t) = \frac{\partial \dot{F}(t)}{\partial t} \left( \left| \ddot{\hat{x}}(w(t), t) \right| + \left| \ddot{\hat{x}}(w(t-1), t-1) \right| \right) \\ + \sum_{k=1}^n \left[ \frac{\partial F(t)}{\partial t} \left( \left| \dot{\hat{x}}(w(t), r_k t) \right| + \left| \dot{\hat{x}}(w(t-1), r_k(t-1)) \right| \right) \right] / P_k^2(t) \\ + [F(t) (|\hat{x}(w(t), t)| + |\hat{x}(w(t-1), t-1)|)] / Q^2(t) \quad (32)$$

where  $\psi(t)/\chi(t)$  are measurement/process noise with covariance  $\zeta/\xi$  and zeros mean and  $w$  is the vector of trainable parameters that is defined as:

$$w = [\theta_1, \dots, \theta_M]^T \quad (33)$$

The training algorithm is explained step-by-step in below.

1) The sigma points are computed as:

$$w_h = w_h + \tilde{w}_h, \quad h = 1, \dots, 2M \quad (34)$$

where  $\tilde{w}_h$  is:

$$\tilde{w}_h = \left(\sqrt{M\pi(t)}\right)^T, \quad h = 1, \dots, M \quad (35)$$

$$\tilde{w}_{h+M} = -\left(\sqrt{M\pi(t)}\right)^T, \quad h = 1, \dots, M \quad (36)$$

where  $\pi$  represents the covariance matrix. 2) For each  $w_h$  in (34), compute the cost function  $v$  as:

$$\begin{aligned} v_h(\tilde{w}_h, t) &= \frac{\partial \dot{F}(t)}{\partial t} \left( \left| \ddot{\hat{x}}(\tilde{w}_h(t), t) \right| + \left| \ddot{\hat{x}}(\tilde{w}_h(t-1), t-1) \right| \right) \\ &+ \sum_{k=1}^n \left[ \frac{\partial F(t)}{\partial t} \left( \left| \dot{\hat{x}}(\tilde{w}_h(t), r_k t) \right| + \left| \dot{\hat{x}}(\tilde{w}_h(t-1), r_k(t-1)) \right| \right) \right] / P_k^2(t) \\ &+ [F(t) (|\hat{x}(\tilde{w}_h(t), t)| + |\hat{x}(\tilde{w}_h(t-1), t-1)|)] / Q^2(t) \end{aligned} \quad (37)$$

3) From (37), compute the mean of  $v_h, h = 1, \dots, 2(M)$  as:

$$v_m = \sum_{h=1}^M v_h / (2M) \quad (38)$$

4) From (38) for the covariance of forecasted measurements ( $\pi_x$ ), one has:

$$\pi_x = \frac{1}{2M} \sum_{h=1}^{2M} (v_h - v_m)^2 + \zeta \quad (39)$$

5) Compute cross-covariance  $\pi_{wx}$  as:

$$\pi_{wx} = \frac{1}{2M} \sum_{h=1}^{2M} (\tilde{w}_h - \hat{w}) (v_h - v_m) \quad (40)$$

where

$$\hat{w} = \frac{1}{2M} \sum_{h=1}^{2M} \tilde{w}_h \quad (41)$$

6) The Kalman gain is obtained as:

$$K(t) = \pi_{wx} \pi_x^{-1} \quad (42)$$

7) Update the vector of parameters  $w$  as:

$$w(t+1) = w(t) - K(t) v_m(t) \quad (43)$$

8) Update the covariance matrix  $\pi$  as:

$$\pi(t+1) = \pi(t) - K(t) \pi_x K^T(t) \quad (44)$$

## V. STABILITY AND CONVERGENCE ANALYSIS

The main results for the stability analysis is summarized in Theorem V:

*Theorem 1: By the proposed adaptation law (43), the dynamic of the convergence error is stable.*

*Proof:*

To stability and convergence analysis the following Lyapunov function is taken to account:

$$V(t) = \left( \begin{array}{c} \ddot{\hat{x}}(\theta(t), t) + \sum_{k=1}^n \dot{\hat{x}}(\theta(t), r_k t) / P_k(t) \\ + \hat{x}(\theta(t), t) / Q(t) - G(t) \end{array} \right)^2 \quad (45)$$

Then time difference of  $V(k)$  in (45), yields:

$$\begin{aligned} V(t) - V(t-1) &= \left( \begin{array}{c} \ddot{\hat{x}}(\theta(t), t) + \sum_{k=1}^n \dot{\hat{x}}(\theta(t), r_k t) / P_k(t) \\ + \hat{x}(\theta(t), t) / Q(t) - G(t) \end{array} \right)^2 \\ &- \left( \begin{array}{c} \ddot{\hat{x}}(\theta(t-1), (t-1)) + \\ \sum_{k=1}^n \dot{\hat{x}}(\theta(t-1), r_k(t-1)) / P_k(t-1) + \\ \hat{x}(\theta(t-1), (t-1)) / Q(t-1) - G(t-1) \end{array} \right)^2 \end{aligned} \quad (46)$$

Considering the fact that sample time is enough small the equation (46) can be simplified as:

$$\begin{aligned} V(t) - V(t-1) &\leq \left| \ddot{\hat{x}}(\theta(t), t) \right|^2 - \left| \ddot{\hat{x}}(\theta(t-1), t-1) \right|^2 \\ &+ \sum_{k=1}^n \left[ \left| \dot{\hat{x}}(\theta(t), r_k t) \right|^2 - \left| \dot{\hat{x}}(\theta(t-1), r_k(t-1)) \right|^2 \right] \\ &/ P_k^2(t) + \left[ \left| \hat{x}(\theta(t), t) \right|^2 - \left| \hat{x}(\theta(t-1), t-1) \right|^2 \right] / Q^2(t) \end{aligned} \quad (47)$$

From (23) and (47), one has:

$$\begin{aligned} &\left| \ddot{\hat{x}}(\theta(t), t) \right|^2 - \left| \ddot{\hat{x}}(\theta(t-1), t-1) \right|^2 \\ &= [\theta(t) - \theta(t-1)]^T \frac{\partial \dot{F}(t)}{\partial t} \left( \begin{array}{c} \left| \ddot{\hat{x}}(\theta(t), t) \right| + \\ \left| \ddot{\hat{x}}(\theta(t-1), t-1) \right| \end{array} \right) \end{aligned} \quad (48)$$

Similarly, from (15) and (47), one has:

$$\begin{aligned} &\left| \dot{\hat{x}}(\theta(t), r_k t) \right|^2 - \left| \dot{\hat{x}}(\theta(t-1), r_k(t-1)) \right|^2 \\ &\leq [\theta(t) - \theta(t-1)]^T \frac{\partial F(t)}{\partial t} \left( \begin{array}{c} \left| \dot{\hat{x}}(\theta(t), r_k t) \right| + \\ \left| \dot{\hat{x}}(\theta(t-1), r_k(t-1)) \right| \end{array} \right) \end{aligned} \quad (49)$$

Also, from (14) and (47), one can writes:

$$\begin{aligned} &\left| \hat{x}(\theta(t), t) \right|^2 - \left| \hat{x}(\theta(t-1), t-1) \right|^2 \\ &\leq [\theta(t) - \theta(t-1)]^T F(t) \left( \left| \hat{x}(\theta(t), t) \right| + \left| \hat{x}(\theta(t-1), t-1) \right| \right) \end{aligned} \quad (50)$$

Then from equations (48-50), the inequality (47), becomes:

$$\begin{aligned}
 &V(t) - V(t-1) \\
 &\leq [\theta(t) - \theta(t-1)]^T \\
 &\quad \cdot \frac{\partial \dot{F}(t)}{\partial t} \left( \left| \ddot{\hat{x}}(\theta(t), t) \right| + \left| \ddot{\hat{x}}(\theta(t-1), t-1) \right| \right) \\
 &\quad + \sum_{k=1}^n \left[ \frac{\partial F(t)}{\partial t} \left( \left| \dot{\hat{x}}(\theta(t), r_k t) \right| + \left| \dot{\hat{x}}(\theta(t-1), r_k(t-1)) \right| \right) \right] / P_k^2(t) \\
 &\quad + \left[ F(t) \left( \left| \dot{\hat{x}}(\theta(t), t) \right| + \left| \dot{\hat{x}}(\theta(t-1), t-1) \right| \right) \right] / Q^2(t) \quad (51)
 \end{aligned}$$

From tuning rules (43), the inequality (51), becomes:

$$\begin{aligned}
 &V(t) - V(t-1) \\
 &\leq -K v_m \\
 &\quad \cdot \left\{ \begin{aligned} &\frac{\partial \dot{F}(t)}{\partial t} \left( \left| \ddot{\hat{x}}(\theta(t), t) \right| + \left| \ddot{\hat{x}}(\theta(t-1), t-1) \right| \right) + \\ &\sum_{k=1}^n \left[ \frac{\partial F(t)}{\partial t} \left( \left| \dot{\hat{x}}(\theta(t), r_k t) \right| + \left| \dot{\hat{x}}(\theta(t-1), r_k(t-1)) \right| \right) \right] / P_k^2(t) \\ &+ \left[ F(t) \left( \left| \dot{\hat{x}}(\theta(t), t) \right| + \left| \dot{\hat{x}}(\theta(t-1), t-1) \right| \right) \right] / Q^2(t) \end{aligned} \right\}^2 \quad (52)
 \end{aligned}$$

From (52), it is realized that  $V(t) - V(t-1) \leq 0$  and then from Laypunov theorem the stability is proved.

VI. SIMULATIONS

In this section the proficiency of the suggested solver is evaluated in two examples. To evaluate the performance of the suggested scenario, the following measures are taken to account.

$$RMSE = \sqrt{\frac{1}{N} \sum_{i=1}^N (x_i - \hat{x}_i)^2} \quad (53)$$

$$VAR = \sum_{i=1}^N (x - \hat{x}_i)^2 / (N - 1) \quad (54)$$

$$TIC = \frac{\sqrt{\frac{1}{N} \sum_{i=1}^N (x_i - \hat{x}_i)^2}}{\sqrt{\frac{1}{N} \sum_{i=1}^N x_i^2} + \sqrt{\frac{1}{N} \sum_{i=1}^N \hat{x}_i^2}} \quad (55)$$

where  $N$  represents the number of data,  $x_i$  is the real solution at  $i$ -th sample,  $\hat{x}_i$  is the estimated solution by T3-FLS at  $i$ -th sample and  $RMSE$ ,  $VAR$  and  $TIC$  represent root-mean-square-error, variance and Theil's inequality coefficient, respectively. □

Example 1: In this example, the following SMDE is considered:

$$\ddot{x}(t) + \frac{1}{t} \dot{x}(t/2) + \frac{1}{t^2} \dot{x}(t/4) + \frac{1}{1-t} x(t) = H(t) \quad 0 < t \leq 1 \quad (56)$$

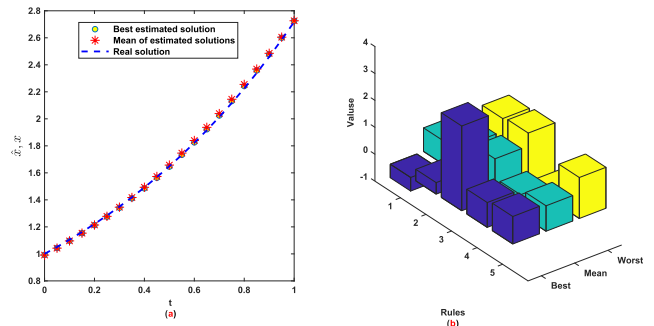


FIGURE 4. Example 1: (a): Solution performance; (b): Rule parameters of T3-FLS.

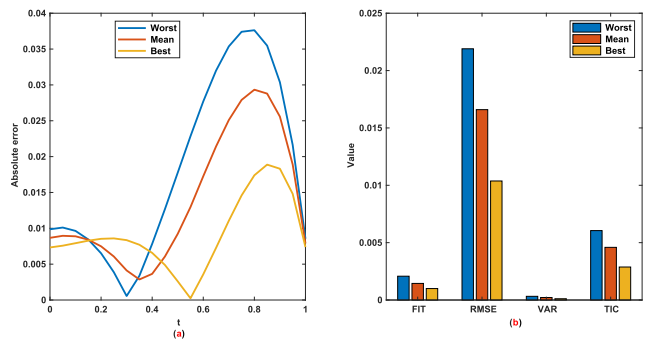


FIGURE 5. Example 1: (a): Trajectories of AE; (b): The values of VAR, FIT, TIC and RMSE.

where

$$H(t) = e^t + \frac{1}{t} e^{t/2} + \frac{1}{t^2} e^{t/4} + \frac{1}{1-t} e^t \quad (57)$$

The number rules is considered to be 10. The centers of MFs are in  $[0, 0.25, \dots, 1]$ . The number of  $\alpha$ -cuts is considered to be 4. After 15 runs the results are presented as follows. The trajectories of the best estimated and real solutions and mean of estimations are given in Fig. 4(a) and the parameters of T3-FLS are given in Fig. 4(b). The trajectory of absolute error (AE) is shown in Fig. 5(a) and values of other indexes are given in Fig. 5(b). The results of statistical analysis for TIC, RMSE, VAR and FIT are depicted in Figs 7- 9. It is observed that the value of RMSE is significantly small and the trajectory of output of T3-FLS  $\hat{x}$  is well converged to the real solution  $x(t) = exp(t)$ .

To better show the robustness and accuracy of the suggested method, the values of interquartile range (IR), mean of AE, median (Med) and minimum (Min) are given in Table 1. It is observed that the values of mean item are in range of  $10^{-3}$  to  $10^{-2}$  and the values of IR item are in the range of  $10^{-3}$ , that indicates an accurate performance.

Example 2: For the second examination, we consider a SMDE as:

$$\ddot{x}(t) + \frac{1}{t} \dot{x}(t/2) + \frac{1}{t^2} \dot{x}(t/4) + \frac{1}{1-t} x(t) = R(t), \quad 0 < t \leq 1 \quad (58)$$

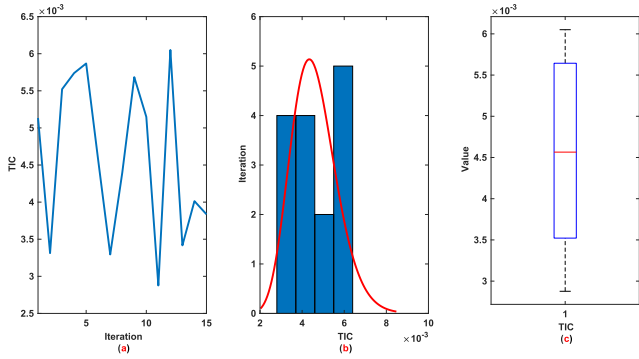


FIGURE 6. Example 1: TIC examination: (a): Trajectory; (b): Histogram; (c): Box plot.

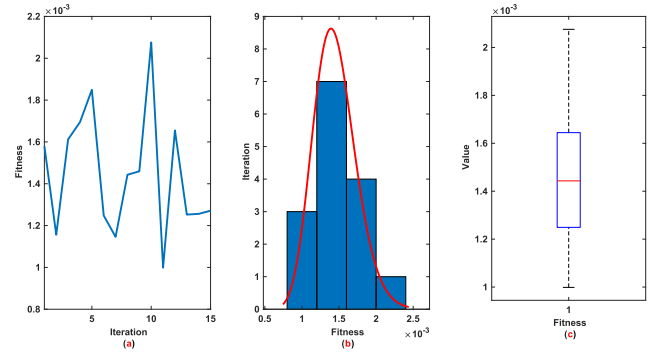


FIGURE 9. Example 1: FIT examination: (a): Trajectory; (b): Histogram; (c): Box plot.

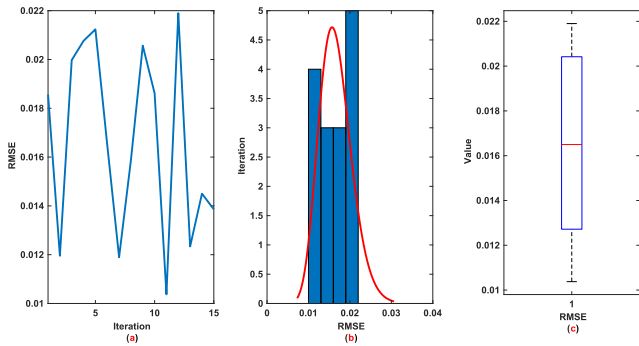


FIGURE 7. Example 1: RMSE examination: (a): Trajectory; (b): Histogram; (c): Box plot.

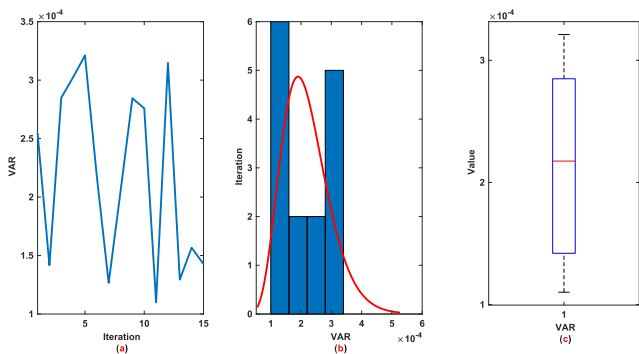


FIGURE 8. Example 1: VAR examination: (a): Trajectory; (b): Histogram; (c): Box plot.

where

$$R(t) = -\frac{1}{t} \sin(t/2) - \frac{1}{t^2} \sin(t/4) + \frac{t}{1-t} \cos(t) \quad (59)$$

The simulation parameters are same as Example 1. After 15 runs the results are presented as follows. The trajectories of the best estimated and real solutions and mean of estimations are given in Fig. 10(a) and the parameters T3-FLS are given in Fig. 10(b). The trajectory of AE is shown in Fig. 11(a) and value of other indexes are given in Fig. 11(b). The results of statistical analysis for FIT, TIC, VAR and RMSE are depicted in Figs 13- 15. It is observed that the value of RMSE is

TABLE 1. Example 1: Statistical analysis.

t	Min	Med	IR	Mean
0	0.0001	0.0026	0.0026	0.0015
0.0500	0.0003	0.0025	0.0024	0.0011
0.1000	0.0003	0.0025	0.0024	0.0018
0.1500	0.0009	0.0028	0.0025	0.0016
0.2000	0.0001	0.0034	0.0031	0.0021
0.2500	0.0004	0.0041	0.0037	0.0031
0.3000	0.0006	0.0050	0.0049	0.0039
0.3500	0.0002	0.0059	0.0061	0.0044
0.4000	0.0007	0.0070	0.0062	0.0046
0.4500	0.0024	0.0083	0.0069	0.0053
0.5000	0.0009	0.0097	0.0090	0.0083
0.5500	0.0009	0.0116	0.0123	0.0122
0.6000	0.0024	0.0149	0.0162	0.0110
0.6500	0.0064	0.0191	0.0201	0.0091
0.7000	0.0108	0.0235	0.0238	0.0068
0.7500	0.0155	0.0278	0.0273	0.0053
0.8000	0.0201	0.0315	0.0316	0.0056
0.8500	0.0241	0.0343	0.0341	0.0045
0.9000	0.0271	0.0356	0.0360	0.0052
0.9500	0.0285	0.0348	0.0352	0.0051
1.0000	0.0263	0.0313	0.0312	0.0045

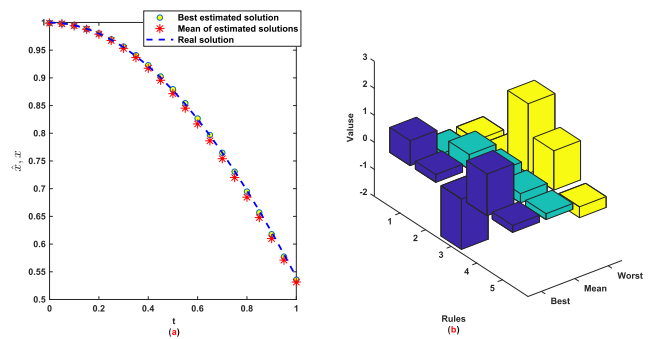


FIGURE 10. Example 2: (a): Solution performance; (b): Rule parameters of T3-FLS.

significantly small and the trajectory of output of T3-FLS  $\hat{x}$  is well converged to the real solution  $x(t) = \cos(t)$ .

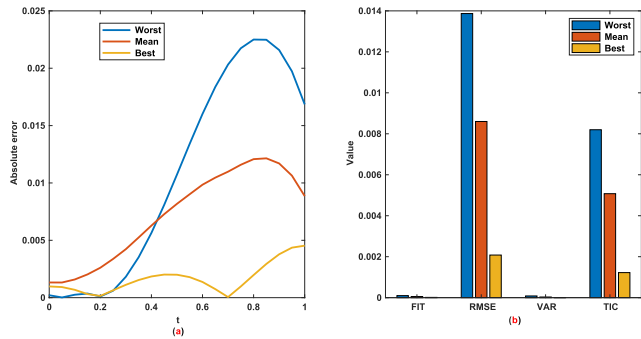


FIGURE 11. Example 2: (a): Trajectories of AE; (b): The values of FIT, TIC, RMSE and VAR.

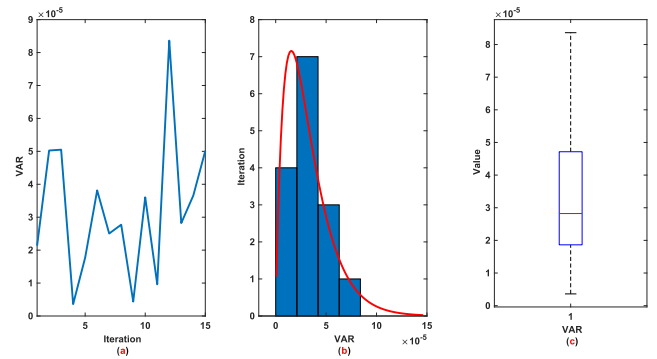


FIGURE 14. Example 2: VAR examination: (a): Trajectory; (b): Histogram; (c): Box plot.

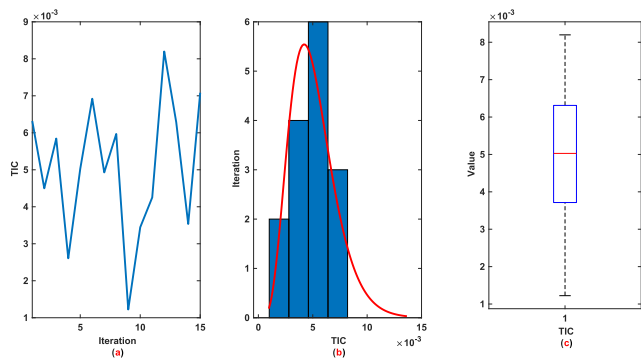


FIGURE 12. Example 2: TIC examination: (a): Trajectory; (b): Histogram; (c): Box plot.

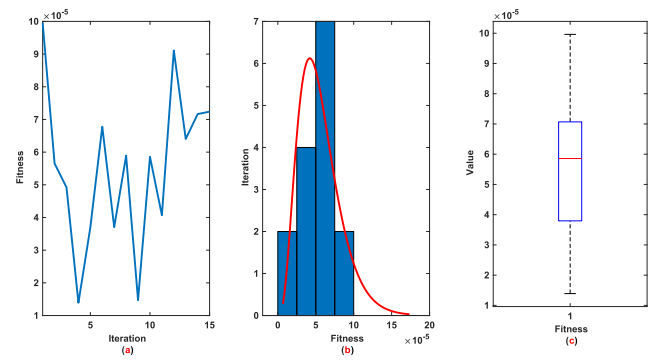


FIGURE 15. Example 2: FIT examination: (a): Trajectory; (b): Histogram; (c): Box plot.

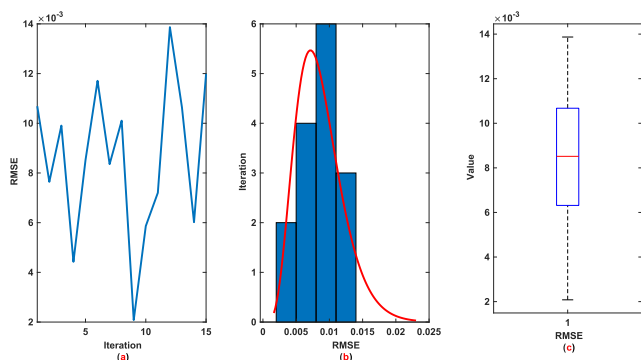


FIGURE 13. Example 2: RMSE examination: (a): Trajectory; (b): Histogram; (c): Box plot.

To better show the robustness and accuracy of the suggested method, the values IR, mean of AE, Med and Min are given in Table 2. It is realized that the values mean item are in range of  $10^{-3}$  to  $10^{-2}$  and the values of IR index are small enough that indicate an accurate solution.

Example 3: In this example a comparison is given to better show the superiority of the suggested scheme. The performance is compared with NN based approach that has been presented in [18]. In [18], NNs and evolutionary based algorithms such as genetic and pattern search algorithms (G-PSAs) are employed to solve PDEs. In this example the method of [18] is applied on the equations of Examples 1–2.

TABLE 2. Example 2: Statistical analysis.

t	Min	Med	IR	Mean
0	0.0000	0.0013	0.0011	0.0015
0.0500	0.0002	0.0012	0.0010	0.0013
0.1000	0.0000	0.0012	0.0011	0.0015
0.1500	0.0001	0.0014	0.0014	0.0017
0.2000	0.0000	0.0018	0.0016	0.0019
0.2500	0.0004	0.0025	0.0022	0.0024
0.3000	0.0006	0.0034	0.0030	0.0026
0.3500	0.0003	0.0046	0.0050	0.0030
0.4000	0.0018	0.0061	0.0062	0.0035
0.4500	0.0027	0.0078	0.0077	0.0046
0.5000	0.0038	0.0095	0.0096	0.0053
0.5500	0.0049	0.0113	0.0115	0.0055
0.6000	0.0061	0.0129	0.0124	0.0056
0.6500	0.0073	0.0142	0.0130	0.0052
0.7000	0.0084	0.0153	0.0151	0.0053
0.7500	0.0093	0.0160	0.0164	0.0054
0.8000	0.0099	0.0161	0.0164	0.0049
0.8500	0.0102	0.0158	0.0159	0.0046
0.9000	0.0100	0.0147	0.0147	0.0039
0.9500	0.0080	0.0130	0.0129	0.0033
1.0000	0.0054	0.0106	0.0105	0.0028

The values of mean of RMSE after 10 epoches are given in Table 3. From Table 3, the superiority the suggested fuzzy

**TABLE 3. Example 3: RMSE comparison for different methods.**

Method	Equation	
	(56)	(58)
NNs & G-PSAs [18]	0.0231	0.0108
T3-FLS & UKF	0.0165	0.0085

based solver is demonstrated. It should be noted that the computational cost of the learning method in [18] is more than the suggested method in this paper.

*Remark 2: Concerning the numerical analysis, the readers can observe the CESTAC method and the CADNA library.*

*Remark 3: In this study only the rule parameters are updated. Then the main drawback is that, the structure is not tuned. For the future studies, the structure optimality of the suggested fuzzy system can be taken into account.*

## VII. CONCLUSION

In this study, a new robust and stable approach using T3-FLS and UKF is presented for solving of SMDEs. Two numerical simulations are given to show the applicability of the suggested solver. The stability is proved by Lyapunov approach. Several statistical examination are provided to show the superiority of the suggested algorithm such as: studding of RMSE, TIC, Interquartile Range and Variance, metrics. It is shown that the values of RMSE in two examples are significantly small and the trajectories of output of FLSs are well converged to the real solutions.

## REFERENCES

- [1] M. S. M. Bahgat, "Approximate analytical solution of the linear and nonlinear multi-pantograph delay differential equations," *Phys. Scripta*, vol. 95, no. 5, May 2020, Art. no. 055219.
- [2] K. Jiang, "Discontinuous Galerkin methods for multi-pantograph delay differential equations," *Adv. Appl. Math. Mech.*, vol. 12, no. 1, pp. 189–211, Jun. 2020.
- [3] N. R. Anakira, A. Jameel, A.-K. Alomari, A. Saaban, M. Almahameed, and I. Hashim, "Approximate solutions of multi-pantograph type delay differential equations using multistage optimal homotopy asymptotic method," *J. Math. Fundam. Sci.*, vol. 50, no. 3, pp. 221–232, 2018.
- [4] M. Bilal, N. Rosli, I. Ahmad, and S. Ullah, "Numerical solution of second order delay type differential equation by collocation method via first boubeker polynomials," *Global J. Pure Appl. Math.*, vol. 13, no. 9, pp. 6571–6582, 2017.
- [5] Y. Yang and E. Tohidi, "Numerical solution of multi-pantograph delay boundary value problems via an efficient approach with the convergence analysis," *Comput. Appl. Math.*, vol. 38, no. 3, p. 127, Sep. 2019.
- [6] E. H. Doha, A. H. Bhrawy, and R. M. Hafez, "Numerical algorithm for solving multi-pantograph delay equations on the half-line using jacobi rational functions with convergence analysis," *Acta Mathematicae Applicatae Sinica, English Ser.*, vol. 33, no. 2, pp. 297–310, Apr. 2017.
- [7] Z. Sabir, J. L. G. Guirao, T. Saeed, and F. Erdoğan, "Design of a novel second-order prediction differential model solved by using adams and explicit Runge–Kutta numerical methods," *Math. Problems Eng.*, vol. 2020, pp. 1–7, Jul. 2020.
- [8] F. Mohammadi, "Numerical solution of systems of fractional delay differential equations using a new kind of wavelet basis," *Comput. Appl. Math.*, vol. 37, no. 4, pp. 4122–4144, Sep. 2018.
- [9] A. Rayal and S. R. Verma, "Numerical analysis of pantograph differential equation of the stretched type associated with fractal-fractional derivatives via fractional order Legendre wavelets," *Chaos, Solitons Fractals*, vol. 139, Oct. 2020, Art. no. 110076.
- [10] K. Li, K. Tang, T. Wu, and Q. Liao, "D3M: A deep domain decomposition method for partial differential equations," *IEEE Access*, vol. 8, pp. 5283–5294, 2020.
- [11] X. Zhang, D. Wang, Z. Zhou, and Y. Ma, "Robust low-rank tensor recovery with rectification and alignment," *IEEE Trans. Pattern Anal. Mach. Intell.*, vol. 43, no. 1, pp. 238–255, Jan. 2019.
- [12] X. Zhang, R. Jiang, T. Wang, and J. Wang, "Recursive neural network for video deblurring," *IEEE Trans. Circuits Syst. Video Technol.*, early access, Nov. 3, 2020, doi: 10.1109/TCSVT.2020.3035722.
- [13] X. Zhang, M. Fan, D. Wang, P. Zhou, and D. Tao, "Top-k feature selection framework using robust 0–1 integer programming," *IEEE Trans. Neural Netw. Learn. Syst.*, early access, Jul. 31, 2020, doi: 10.1109/TNNLS.2020.3009209.
- [14] X. Zhang, T. Wang, J. Wang, G. Tang, and L. Zhao, "Pyramid channel-based feature attention network for image dehazing," *Comput. Vis. Image Understand.*, vols. 197–198, Aug. 2020, Art. no. 103003. [Online]. Available: <http://www.sciencedirect.com/science/article/pii/S1077314220300709>
- [15] C.-H. Chou, P.-T. Chen, C.-J. Yang, and K. D. Huang, "Functionalization of wireless control and fuzzy systems to hybrid mini-loaders," *IEEE Access*, vol. 8, pp. 80914–80921, 2020.
- [16] C.-L. Hwang, H. B. Abebe, B.-S. Chen, and F. Wu, "Fuzzy adaptive finite-time cooperative control with input saturation for nonlinear multiagent systems and its application," *IEEE Access*, vol. 8, pp. 105507–105520, 2020.
- [17] J. Yu, W. Xing, Q. Li, J. Wang, and C. Han, "Guaranteed cost consensus for fuzzy multi-agent systems with switching topologies," *IEEE Access*, vol. 8, pp. 50497–50506, 2020.
- [18] M. A. Z. Raja, "Numerical treatment for boundary value problems of pantograph functional differential equation using computational intelligence algorithms," *Appl. Soft Comput.*, vol. 24, pp. 806–821, Nov. 2014.
- [19] M. A. Z. Raja, I. Ahmad, I. Khan, M. I. Syam, and A. M. Wazwaz, "Neuro-heuristic computational intelligence for solving nonlinear pantograph systems," *Frontiers Inf. Technol. Electron. Eng.*, vol. 18, no. 4, pp. 464–484, Apr. 2017.
- [20] C. Hou, T. E. Simos, and I. T. Famelis, "Neural network solution of pantograph type differential equations," *Math. Methods Appl. Sci.*, vol. 43, no. 6, pp. 3369–3374, Apr. 2020.
- [21] M. A. Z. Raja, J. A. Khan, S. M. Shah, R. Samar, and D. Behloul, "Comparison of three unsupervised neural network models for first Painlevé transcendent," *Neural Comput. Appl.*, vol. 26, no. 5, pp. 1055–1071, Jul. 2015.
- [22] M. A. Z. Raja, R. Samar, T. Haroon, and S. M. Shah, "Unsupervised neural network model optimized with evolutionary computations for solving variants of nonlinear MHD Jeffery–Hamel problem," *Appl. Math. Mech.*, vol. 36, no. 12, pp. 1611–1638, Dec. 2015.
- [23] F. Jin, J. Liu, H. Chen, and R. Langari, "Interval type-2 trapezoidal fuzzy decision-making method with consistency-improving algorithm and DEA model," *IEEE Access*, vol. 8, pp. 120456–120472, 2020.
- [24] N. F. Jamin, N. M. A. Ghani, and Z. Ibrahim, "Movable payload on various conditions of two-wheeled double links wheelchair stability control using enhanced interval type-2 fuzzy logic," *IEEE Access*, vol. 8, pp. 87676–87694, 2020.
- [25] J. Zheng, W. Du, I. Nascu, Y. Zhu, and W. Zhong, "An interval type-2 fuzzy controller based on data-driven parameters extraction for cement calciner process," *IEEE Access*, vol. 8, pp. 61775–61789, 2020.
- [26] T.-L. Le, T.-T. Huynh, and S.-K. Hong, "Self-organizing interval type-2 fuzzy asymmetric CMAC design to synchronize chaotic satellite systems using a modified grey wolf optimizer," *IEEE Access*, vol. 8, pp. 53697–53709, 2020.
- [27] A. Mohammadzadeh and O. Kaynak, "A novel general type-2 fuzzy controller for fractional-order multi-agent systems under unknown time-varying topology," *J. Franklin Inst.*, vol. 356, no. 10, pp. 5151–5171, Jul. 2019.
- [28] H.-L. Chen, G. Wang, C. Ma, Z.-N. Cai, W.-B. Liu, and S.-J. Wang, "An efficient hybrid kernel extreme learning machine approach for early diagnosis of Parkinson's disease," *Neurocomputing*, vol. 184, pp. 131–144, Apr. 2016.

- [29] L. Hu, G. Hong, J. Ma, X. Wang, and H. Chen, "An efficient machine learning approach for diagnosis of paraquat-poisoned patients," *Comput. Biol. Med.*, vol. 59, pp. 116–124, Apr. 2015.
- [30] C. Li, L. Hou, B. Y. Sharma, H. Li, C. Chen, Y. Li, X. Zhao, H. Huang, Z. Cai, and H. Chen, "Developing a new intelligent system for the diagnosis of tuberculous pleural effusion," *Comput. Methods Programs Biomed.*, vol. 153, pp. 211–225, Jan. 2018.
- [31] L. Shen, H. Chen, Z. Yu, W. Kang, B. Zhang, H. Li, B. Yang, and D. Liu, "Evolving support vector machines using fruit fly optimization for medical data classification," *Knowl.-Based Syst.*, vol. 96, pp. 61–75, Mar. 2016.
- [32] M. Wang and H. Chen, "Chaotic multi-swarm whale optimizer boosted support vector machine for medical diagnosis," *Appl. Soft Comput.*, vol. 88, Mar. 2020, Art. no. 105946. [Online]. Available: <https://www.scopus.com/inward/record.uri?eid=2-s2.0-85076535070&doi=10.1016%2fj.asoc.2019.105946&partnerID=40&md5=8a1c5e7662f93045d36cfacc01b68af2>
- [33] M. Wang, H. Chen, B. Yang, X. Zhao, L. Hu, Z. Cai, H. Huang, and C. Tong, "Toward an optimal kernel extreme learning machine using a chaotic moth-flame optimization strategy with applications in medical diagnoses," *Neurocomputing*, vol. 267, pp. 69–84, Dec. 2017.
- [34] X. Xu and H.-L. Chen, "Adaptive computational chemotaxis based on field in bacterial foraging optimization," *Soft Comput.*, vol. 18, no. 4, pp. 797–807, Apr. 2014.
- [35] Y. Xu, H. Chen, J. Luo, Q. Zhang, S. Jiao, and X. Zhang, "Enhanced moth-flame optimizer with mutation strategy for global optimization," *Inf. Sci.*, vol. 492, pp. 181–203, Aug. 2019.
- [36] R. Costanzi, F. Fanelli, E. Meli, A. Ridolfi, A. Caiti, and B. Allotta, "UKF-based navigation system for AUVs: Online experimental validation," *IEEE J. Ocean. Eng.*, vol. 44, no. 3, pp. 633–641, Jul. 2019.
- [37] G. Hu, B. Gao, Y. Zhong, and C. Gu, "Unscented Kalman filter with process noise covariance estimation for vehicular INS/GPS integration system," *Inf. Fusion*, vol. 64, pp. 194–204, Dec. 2020.
- [38] G. Hu, W. Wang, Y. Zhong, B. Gao, and C. Gu, "A new direct filtering approach to INS/GNSS integration," *Aerosp. Sci. Technol.*, vol. 77, pp. 755–764, Jun. 2018.
- [39] A. Iserles and Y. Liu, "On pantograph integro-differential equations," *J. Integral Equ. Appl.*, vol. 6, no. 2, pp. 213–237, Jun. 1994.
- [40] L. Qiu, T. Mitsui, and J.-X. Kuang, "The numerical stability of the  $\theta$ -method for delay differential equations with many variable delays," *J. Comput. Math.*, vol. 7, pp. 523–532, Sep. 1999.
- [41] H. Brunner, "Collocation methods for pantograph-type volterra functional equations with multiple delays," *Comput. Methods Appl. Math.*, vol. 8, pp. 207–222, Jan. 2008.

• • •